Geomorphology 412 (2022) 108318

Contents lists available at ScienceDirect

Geomorphology

journal homepage: www.journals.elsevier.com/geomorphology

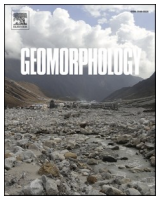

Spatial and temporal trends in California coastal cliff retreat

Zuzanna M. Swirad [a,b,*], Adam P. Young [a]

[a] Scripps Institution of Oceanography, University of California San Diego, 9500 Gilman Dr., La Jolla, CA 92093, USA
[b] Institute of Geophysics, Polish Academy of Sciences, ul. Księcia Janusza 64, 01-452 Warszawa, Poland

ARTICLE INFO

Keywords:
Coastal cliffs
Cliff erosion
LiDAR
California coast

ABSTRACT

Airborne LiDAR datasets were used to measure erosion and retreat along 866 km of California coastal cliffs between 2009–2011 and 2016. Erosion exceeding the level of detection was observed at 55% of cliffs. State-averaged cliff face and top retreat rates were both 0.06 m yr^{-1}, and varied alongshore, with more erosion in northern California compared to southern and central California. Retreat rates were higher for unarmored cliffs and cliffs fronted by sandy beaches. Mean cliff top retreat rates were lower than in previous studies conducted between the 1920s–1930s and 1998/2002, and between 1998 and 2009–2011. However, the average cliff face retreat rates and statistical distributions were similar ($r^2 = 0.99$) for the 1998 to 2009–2011 and 2009–2011 to 2016 time periods. No significant correlation was found between cliff erosion rates and environmental factors such as rock hardness, rainfall, groundwater, waves, and relative sea level change. However, the highest cliff face retreat rates (>1 m yr^{-1}) occurred at locations with weak rocks.

1. Introduction

Rocky coasts are erosional environments found around the world (Emery and Kuhn, 1982; Young and Carilli, 2019). Understanding the rates and controls of cliff erosion is critical for building more resilient communities. Future sea level rise is expected to increase the rates of cliff erosion (Dickson et al., 2007), but the quantitative relationships between erosional drivers and rock coast change are poorly constrained. Understudied compared to soft sediment coasts (Naylor et al., 2010), rock coasts have received increased scientific interest over the last 20 years with advances in high-resolution monitoring (Rosser et al., 2013; Williams et al., 2018; Young et al., 2021), exploratory numerical modelling (Kline et al., 2014; Limber et al., 2014; Matsumoto et al., 2016) and millennial-scale reconstruction (Regard et al., 2012; Hurst et al., 2016; Swirad et al., 2020) of erosion.

Cliffs are present along the majority of California's 1646 km coastline (Griggs et al., 2005) and their erosion threatens critical infrastructure such as highways, railways, wastewater facilities, military bases, universities, and residential structures, and public resources including numerous state parks (Young, 2018). Recent coastal cliff failures have caused fatalities (Perry, 2000. January 16; Gross and Davis, 2008. August 21; Evans, 2015. Mar 26) and significant infrastructure damage (Thomas and Loague, 2014; Warrick et al., 2019). Erosion rates vary alongshore with some locations experiencing repetitive high magnitude cliff failures such as Daly City, Portuguese Bend, and San Onofre (Hapke et al., 2009; Young et al., 2009; Young, 2015, 2018). There is a high diversity in driving forces (waves, rainfall, earthquakes), magnitude of erosion, and impact on society (Griggs et al., 2005).

Three large-scale quantitative studies of California cliff retreat now exist. Hapke et al. (2009) measured cliff top retreat by comparing 1920s–1930s topographic maps and 1998/2002 LiDAR datasets for 353 km of cliffs spread throughout the state (20% of the California coast) and found generally higher retreat rates in northern and central California (0.2–0.7 m yr^{-1}) compared to southern California (0.2–0.3 m yr^{-1}). Young (2018) used 1998 and 2009–2011 LiDAR datasets to measure cliff erosion and cliff face and top retreat rates for 595 km of the southern and central California coastline (35% of the California coast), and found higher retreat rates for cliffs fronted by sandy beaches (0.06 m yr^{-1}) than those without a beach (0.04 m yr^{-1}). Swirad and Young (2021) used 2009–2011 and 2016 LiDAR datasets to measure cliff erosion for 866 km (53%) of the California coastline, identified landslide volume frequency relationships, and quantified state- and county-averaged cliff face retreat rates.

Sunamura (1992) suggested that marine coastal cliff erosion occurs when the assailing wave force exceeds rock resistance. Rock resistance is a function of mechanical strength dictated by lithology and structure. Rock strength is reduced by weathering processes. Wave force includes the effect of mechanical, hydraulic, and pneumatic action of waves

* Corresponding author at: Scripps Institution of Oceanography, University of California San Diego, 9500 Gilman Dr., La Jolla, CA 92093, USA.
E-mail address: zswirad@igf.edu.pl (Z.M. Swirad).

https://doi.org/10.1016/j.geomorph.2022.108318
Received 8 February 2022; Received in revised form 17 May 2022; Accepted 19 May 2022
Available online 25 May 2022

impacting a cliff, controlled by offshore wave conditions and wave transformation (a function of tides, beach morphology, etc.) at the nearshore and foreshore (Sunamura, 1992). Naylor and Stephenson (2010) suggested rock coasts are threshold-dominated environments where erosion events only occur once a certain threshold is reached. Kline et al. (2014) explored the threshold depth of a wave-cut notch leading to the failure of the overhanging upper cliff, while Brooks et al. (2012) established marine and subaerial process thresholds associated with high magnitude cliff erosion events. In addition to marine-related processes, coastal cliffs also experience erosion processes similar to terrestrial hillslopes where mass movements occur as a function of topography, geology, tectonics, hydrology, precipitation, land cover, and human action (Reichenbach et al., 2018).

Direct quantitative relationships between cliff erosion and controlling factors are difficult to constrain because of lagged responses, the complexity of processes, co-occurrence of drivers, and difficulties in measuring rock coast change at the appropriate scale and frequency (Trenhaile, 1987). Despite the general understanding of what drives coastal change (i.e. waves, rainfall), it remains challenging to predict cliff erosion at specific locations and times because of the wide range of erosional processes, variable temporal changes and processes, geomorphic feedbacks, and highly variable geologic, oceanographic, and climatic settings (Young, 2018). Recent advances in 3D laser scanning and Structure-from-Motion photogrammetry allow high-resolution repeat surveys of coastal cliff morphology that can provide insight into erosion processes including rockfall sequencing (Rosser et al., 2013), statistical distributions of cliff change (Young et al., 2011; Barlow et al., 2012), the importance of cliff face geometry (Lim et al., 2010), lithologic influence (Collins and Sitar, 2008), and wave impacts on the cliff base (Young et al., 2021).

This study builds on previous research (Young, 2018) to explore spatio-temporal cliff erosion patterns using datasets initially developed by Swirad and Young (2021) for the California coast. We analyze alongshore variability of cliff face and top retreat rates and potential influencing factors. To explore temporal patterns, the recent cliff retreat rates from Swirad and Young (2021) spanning ~6 years are compared with two historical datasets (Hapke et al., 2009; Young, 2018) of different timespans (~70 and ~12 years).

2. Study area

The California coast (Fig. 1) is tectonically active with a series of fault zones dividing the North American and Pacific plates. Topographic expression of the tectonic activity includes several coastal mountain ranges (Coast Ranges, Transverse Ranges, and Peninsular Ranges) and a series of uplifted marine terraces (Griggs et al., 2005). Rock types vary at local to regional scales, including a range of igneous and sedimentary lithologies of varied age that are often overlaid by Quaternary sedimentary deposits (Jennings, 1977; Hapke et al., 2014). The coastal cliffs are usually fronted by sandy and/or cobble beaches, but plunging cliffs and cliffs fronted by exposed rocky shore platforms also exist (Griggs et al., 2005). Beach morphology (width, height) varies widely in space and time (Vos et al., 2020).

The California climate is characterized by dry summers and occasionally wet winters with the majority (e.g. 76–84% in San Diego, San Francisco and Eureka) of rainfall occurring between November and March. Rainfall generally increases northwards with annual rainfall ranging from 257 mm in San Diego to 1798 mm in Crescent City (wrcc.dri.edu). The study time period includes the very strong 2015–2016 El Niño and associated coastal impacts (Ludka et al., 2016; Barnard et al., 2017; Young et al., 2018; Smith and Barnard, 2021). California receives locally generated waves and waves from both hemispheres in the Pacific Ocean. The wave climate is seasonal with dominant winter waves from the northern Pacific and summer southern hemisphere swell. Wave conditions vary alongshore with average offshore buoy significant wave height (ndbc.noaa.gov) of 1.2–1.3 m in southern (USA/Mexico border to Point Conception; 0–420 km), and 2.2–2.3 m in central (Point Conception to Bodega Head; 420–1132 km) and northern (north of Bodega Head; 1132–1646 km) California. The tides range about 1.6–2.1 m (tidesandcurrents.noaa.gov).

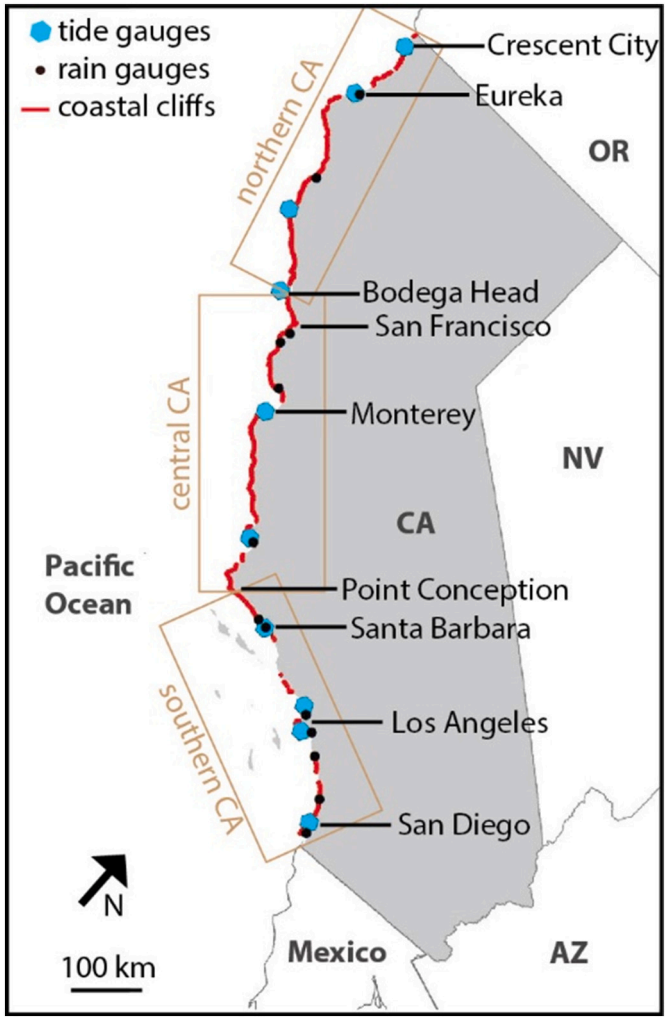

Fig. 1. California study area and distribution of coastal cliffs, tide gauges, and rain stations used in this study.

3. Methods

3.1. Overview of Swirad and Young (2021)

Swirad and Young (2021) used airborne LiDAR datasets collected in 2009–2011 and 2016 to generate 1 m resolution digital elevation models (DEMs) of the California coast. Coastal cliff base and top positions were automatically identified on cross-shore transects spaced 5 m alongshore (Swirad and Young, 2022) and used to delimit the cliff face polygons for change detection analysis. A change raster was created by differencing DEMs, and change objects with vertical change ≥0.62 m and with a horizontal footprint of ≥10 m^2 were identified for cliff faces only. Cliff erosion and deposition change objects were separated from other changes such as noise or vegetation loss/growth using the Normalized Difference Vegetation Index (NDVI) and machine learning methods. The final inventory included 45,699 erosion and 1728 deposition objects (e.g. Fig. 2), each characterized by the surface area and volume of change (Swirad and Young, 2021).

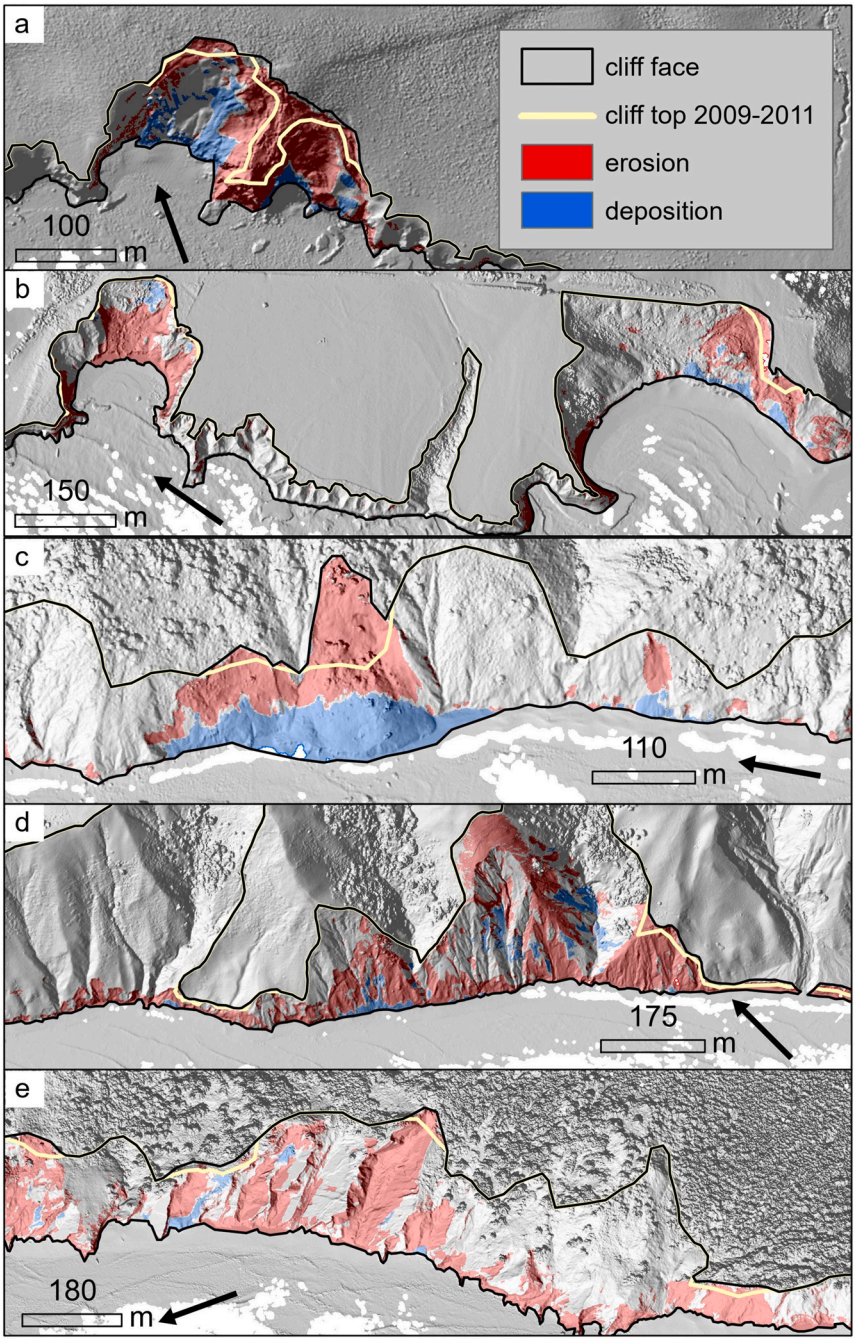

Fig. 2. Examples of change detection near a) Point Arguello (alongshore location 492 km), b) Martin's Beach (952 km), c) Usal Beach (1353 km), d) King Range (1417 km), and e) Centerville Beach area (1459 km).

3.2. Coastal setting, armoring, and morphology

The California coast was divided into 329,123 compartments extending 5 m alongshore and 2 km cross-shore (Young, 2018). Each compartment was ascribed a general coastal setting (rocky coast, cliff fronted by beach, sandy beach, beach backed by marsh/lagoon, bay/harbor) using the classification of Young (2018), Google Earth, and the LiDAR datasets. Rocky coasts included cliffs fronted by shore platforms, rock deposits, and plunging cliffs. Armoring status was mapped by combining the 2010 state of armoring (Young, 2018) and updated armoring data from the California Coastal Commission (provided in Jan 2021).

The cliff face region within each compartment was defined using cliff face polygons developed by Swirad and Young (2021). Cliff morphology was characterized using digital elevation models (DEMs) and slope raster values within the cliff face for each compartment. Cliff base elevation was the lowest 2009–2011 DEM value, cliff height was the difference between the highest and lowest 2009–2011 DEM value, and cliff slope was the mean 2009–2011 slope raster value.

3.3. Cliff erosion and retreat rate, and cliff top hazard index

The cliff change objects were intersected with the compartments to evaluate negative and positive alongshore cliff changes for each compartment. The cliff face retreat rate was calculated as net eroded volume (erosion – deposition)/ cliff height/ 5 m alongshore width/ timespan. Negative retreat values indicate compartments with net accretion. The lower cliff face retreat was calculated for cliff elevations

below the estimated highest total water level (4.7 m NAVD88) during the monitoring period. Cliff top retreat rate was calculated as the area of cliff top loss within each compartment/ 5 m alongshore width/ timespan.

Over long time periods, cliff top and face retreat rates tend to converge. But over shorter timescales they may vary substantially, providing information on geomorphic change and slope stability (Young et al., 2009). Following Young et al. (2009), a cliff top hazard index was estimated by differencing the cliff top and cliff face retreat rates. Positive index values indicate cliff steepening and increasing cliff top instability. Conversely, negative index values indicate faster cliff top retreat compared to the cliff face, overall cliff flattening, and decreasing cliff top instability.

3.4. Historical erosion rates

Young (2018) evaluated cliff change for two preceding time periods (time period 1: 1920s–1930s to 1998/2002, and time period 2: 1998 to 2009–2011) at 5 m alongshore resolution, which was compared to the 2009–2011 to 2016 (time period 3) dataset developed for this study. For time period 1, cliff top retreat rates were measured using Hapke et al. (2009) cliff top lines for 353 km of coastline spanning several regions of California. For time period 2, Young (2018) evaluated cliff face and top retreat rates, and the cliff top hazard index for southern and central California (alongshore locations 0–1137 km).

3.5. Environmental factors

In total, 892 non-zero in situ cliff rock strength measurements were obtained with Proceq Schmidt hammers (Type L and N) at the cliff base using the ASTM method (mean value of ten measurements with outliers removed; ASTM, 2013). Type N hammer measurements were converted to Type L for consistency (Young, 2018). For each compartment, the Schmidt hammer rebound value (R-value) was derived from the nearest measurement located within 100 m. Katz et al. (2000) found a strong relationship (Eq. (1), $r^2 = 0.96$) between R-value and uniaxial compressive strength (UCS) for rock types similar to the California coastline.

$$UCS = 2.208e^{0.067N} \quad (1)$$

We used this relationship to estimate UCS and explore cliff face retreat rates in the context of a global cliff retreat database (Prémaillon et al., 2018) for weak (UCS <25 MPa), medium (25–50 MPa) and hard (≥50 MPa) rocks (classified after Hoek and Brown, 1997).

Daily precipitation data (wrcc.dri.edu, accessed: 2021-3-11) from 13 coastal weather stations spread across the study area (Fig. 1) were used to evaluate total rainfall (mm) over the 2009–2011 to 2016 study period, which was linearly interpolated alongshore. All stations had <5% of missing daily data.

The NASA National Land Data Assimilation Systems (NLDAS) provides modeled groundwater conditions. The NLDAS Mosaic Land Surface Model L4 Monthly, 0.125 × 0.125 degree V002 (disc.gsfc.nasa.gov/datasets/NLDAS_MOS0125_M_002/summary, accessed: 2021-8-25) was used to calculate mean and maximum monthly subsurface runoff (baseflow in kg m^{-2}) for the study period. Each compartment was characterized with the closest runoff value.

Hourly total water levels (TWL, sum of water level and wave runup) were used to estimate wave conditions at the cliff base. Observed hourly water level data (tidesandcurrents.noaa.gov, accessed: 2021-1-7) at ten tidal stations spread across the study area (Fig. 1) were linearly interpolated alongshore. Modeled hourly wave conditions at virtual buoys in ~10 m water depth, estimated with a spectral refraction wave model initialized using offshore buoy data that accounts for bathymetry, beach orientation and wave exposure (O'Reilly et al., 2016), were obtained at 100 m alongshore intervals (CDIP, cdip.ucsd.edu; accessed: 2021-1-13). The deep-water wavelength, L_0, was calculated using the linear dispersion relationship, and the deep-water wave height, H_0, was calculated by reverse shoaling using linear wave theory (USACE, 2015). For cliffs fronted by sandy beaches (403 km), *R2%* wave runup, (i.e. 2% exceedance level of water-level elevation maxima during wave up-rushes), was calculated using Eq. (2) (Stockdon et al., 2006).

$$R2\% = 0.043\sqrt{H_0 L_0} \quad (2)$$

Each compartment used TWL calculated from the nearest virtual buoy and an idealized cliff base elevation of 2.5 m NAVD88 to evaluate three wave-cliff impact metrics of wave impact duration (Eq. (3)), height (Eq. (4)) and height squared (Eq. (5)) (Young et al., 2021).

$$\text{Wave impact duration} = \Sigma \text{ hours TWL} > \text{cliff base} \quad (3)$$

$$\text{Wave impact height} = \Sigma\,(\text{TWL} - \text{cliff base})_{>0} \quad (4)$$

$$\text{Wave impact height squared} = \Sigma\left((\text{TWL} - \text{cliff base})_{>0}{}^2\right) \quad (5)$$

The relative sea level trend was obtained from the ten tidal stations (Fig. 1; derived from mean monthly sea level data, records 43–98 years in length from tidesandcurrents.noaa.gov, accessed: 2021-9-1), and interpolated alongshore.

4. Results

4.1. Coastal setting, armoring, and morphology

About 1065 km (65%) of the California coast contains coastal cliffs, with 45% of these cliffs fronted by sandy beaches. Beaches without cliffs occupy 535 km (33% of the coastline), while 46 km (2.8%) of the coastline consists of harbors and bays. 257 km (16%) of the California coastline is armored, including 104 km (9.8%) of coastal cliffs. Cliff armoring is more common in southern California (20% of cliffs) compared to central (7.1%) and northern (1.5%) California (Fig. 3b).

This study analyzed 866 km of coastal cliffs (53% of the California coastline) where sufficient quality topographic data existed to confidently detect change (Swirad and Young, 2021). The average cliff base elevation was 2.8 ± 1.1 m (mean ± std. dev) NAVD88. Cliff height averaged 42 ± 41 m (mean ± std. dev) NAVD88 and ranged up to 376 m NAVD88 in the King Range (Fig. 3c). Cliff slope averaged 40 ± 10° (mean ± std. dev) with the maximum of 82° (Fig. 3d).

4.2. Cliff erosion, cliff face and top retreat, and cliff top hazard index

Between 2009–2011 and 2016 erosion exceeding detection thresholds occurred along 475 km (55% of the analyzed cliffs), while 8.3 km (1%) experienced net cliff face accretion (volume deposited from adjacent compartments exceeding removed material). The average cliff face retreat rate was 0.06 ± 0.19 m yr^{-1} (mean ± std. dev) with a maximum of 4.7 m yr^{-1} at Centerville Beach (Fig. 4a; Table 1). 7 km of cliffs experienced >1 m yr^{-1} cliff face retreat rates. Armored cliff faces (8.2% analyzed cliffs) retreated twice slower than unarmored cliff sections. 69% of armored cliffs experienced no erosion, compared to 43% of unarmored cliffs. Cliffs fronted by beaches retreated twice faster than cliffs without beaches (Table 2; Fig. 5a).

The average lower cliff face retreat rate was −0.01 ± 0.51 m yr^{-1} (mean ± std. dev) and ranged from −22 m yr^{-1} (accretion) to 2.0 m yr^{-1}. 32% of the lower cliff faces experienced net erosion and 2.2% experienced net accretion (Fig. 4c).

Between 2009–2011 and 2016 cliff top retreat was detected along 87 km (10% of analyzed cliffs) and averaged 0.06 ± 0.43 m yr^{-1} (mean ± std. dev, Table 1) with a maximum of 25 m yr^{-1} at Usal Beach (Fig. 2c). 12 km cliffs experienced >1 m yr^{-1} cliff top retreat. Cliff top retreat hotspots (rates >5 m yr^{-1}) included Palos Verdes, 2.3 km south of Point Arguello, Big Sur, Martin's Beach, Usal Beach, several locations in King

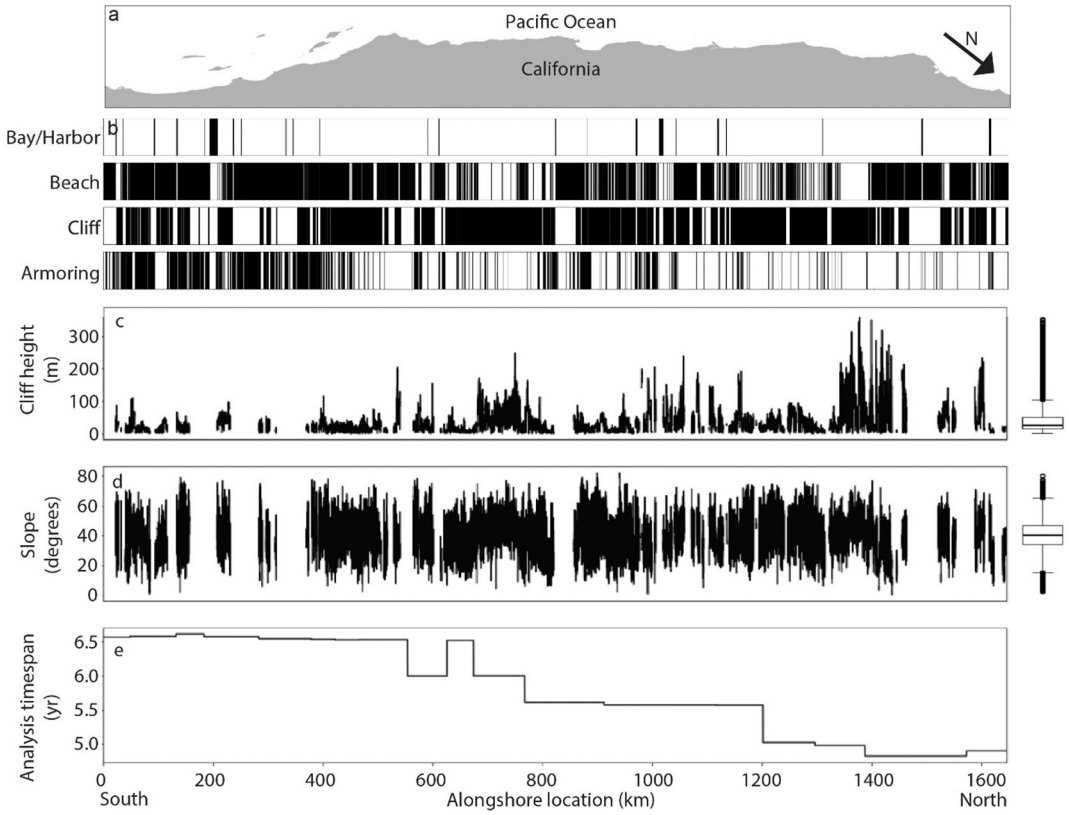

Fig. 3. a) Map of the California coast and alongshore b) coastal setting, c) cliff height, d) average cliff slope, and e) analysis timespan. Boxplots include medians (thick bars), 25th (q1) and 75th (q3) percentiles (boxes), ranges excluding outliers (whiskers), and outliers (circles). Outliers are defined as values greater than q3 + 1.5 × (q3 − q1) or less than q1–1.5 × (q3 − q1). Alongshore locations 0 and 1646 km represent the Mexico (south) and Oregon (north) borders.

Range, Centerville Beach, McNeil Creek area north of Trinidad Head, and a location 3 km north of the Klamath River (Fig. 4d).

85% compartments experienced cliff face retreat rate of <0.1 m yr^{-1} and 92% compartments experienced cliff top retreat rate of <0.1 m yr^{-1} (Fig. 6a). A weak correlation ($r^2 = 0.17$; $p < 0.05$) exists between cliff face and top retreat rates for unarmored cliffs at 5 m alongshore resolution, but it becomes stronger using the alongshore moving average (max $r^2 = 0.68$ at 100 km; $p < 0.05$).

The cliff top hazard index ranged from −24 to 4.7 m yr^{-1} with an average of 0 ± 0.39 m yr^{-1} (mean ± std. dev). 9% of unarmored cliffs experienced cliff flattening and 50% experienced cliff steepening between 2009–2011 and 2016. Locations with high hazard index values (based on time period 3) include Portuguese Bend, Martin's Beach, Point Reyes, Double Point, Caspar Beach, and Centerville Beach (Fig. 4e).

4.3. Temporal comparison

96% of cliffs evaluated in time period 1 experienced cliff top retreat (Fig. 5c). Cliff top retreat rate averaged 0.26 ± 0.31 m yr^{-1} (mean ± std. dev) with a maximum of 3.9 m yr^{-1} (Tables 1 and 2; Hapke et al., 2009). Compared to time period 3, 88% of cliffs retreated faster and 8% retreated slower in time period 1.

55% of cliff top positions considered in time period 2 experienced retreat (Fig. 5c). Cliff top retreat rate averaged 0.12 ± 0.24 m yr^{-1} (mean ± std. dev) with a maximum of 4.2 m yr^{-1} (Tables 1 and 2; Young, 2018). Compared to time period 3, 49% cliffs retreated faster and 12% retreated slower in time period 2.

44% cliffs analyzed in time period 2 experienced cliff face erosion exceeding detection thresholds (Fig. 5d; Young, 2018). The average cliff face retreat rate was 0.04 ± 0.14 m yr^{-1} (mean ± std. dev) and ranged from −0.67 m yr^{-1} (accretion) to 3.9 m yr^{-1} (Tables 1 and 2). When considering only the overlapping cliff sections, cliff face retreat rates in time periods 2 and 3 were similar (mean 0.06 m yr^{-1}), with 37% compartments with higher, and 35% with lower retreat rates than in time period 3. The statistical distribution of cliff face retreat rates for time periods 2 and 3 both show 50% of rates ≤0.005 m yr^{-1}, 75% of rates ≤0.05 m yr^{-1}, 95% of rates ≤0.25 m yr^{-1}, and 99% of rates ≤0.87 m yr^{-1} (Fig. 5d).

At 5 m alongshore resolution, cliff face retreat in time periods 2 and 3 was not well correlated ($n = 80{,}498$; $r^2 = 0.07$, $p < 0.05$; Fig. 6b). However, the correlation increases slightly for larger spatial scales using alongshore smoothing although it remains weak (max $r^2 = 0.25$ at 10 km spatial resolution; $p < 0.05$). Only weak correlations exist between cliff top retreat rates at any combination of time periods and alongshore averaging ($r^2 < 0.05$, $p < 0.05$; Fig. 6d-f), apart from a relationship between time periods 1 and 3 using 10 km ($r^2 = 0.13$; $p < 0.05$) and 100 km ($r^2 = 0.24$; $p < 0.05$) moving average windows.

Locations with relatively high hazard indices (>0.2 m yr^{-1}) in time period 2 and high cliff top retreat rates >1 m yr^{-1} in time period 3 include Pacifica, Bolinas, Double Point, and the northern part of Point Reyes National Seashore (Fig. 6c). However, there was no overall observed relationship between time period 2 cliff top hazard indices and time period 3 cliff top retreat rates.

4.4. Environmental factors

Non-zero Schmidt hammer rebound values (R-values) evaluated for 66 km of cliffs averaged 29 ± 14 (mean ± std. dev) and ranged from 6 to 75 (Fig. 4f), equivalent to UCS of 27 ± 40 MPa (mean ± std. dev) and range of 3.3–356 MPa. R-values varied alongshore but were consistently relatively low in San Diego County (Table 1; Fig. 4f). Weak cliff faces (47 km) retreated twice faster than hard (9.4 km) and medium hardness (10 km) cliffs (Table 2; Fig. 5b).

Total rainfall between the LiDAR surveys generally increased

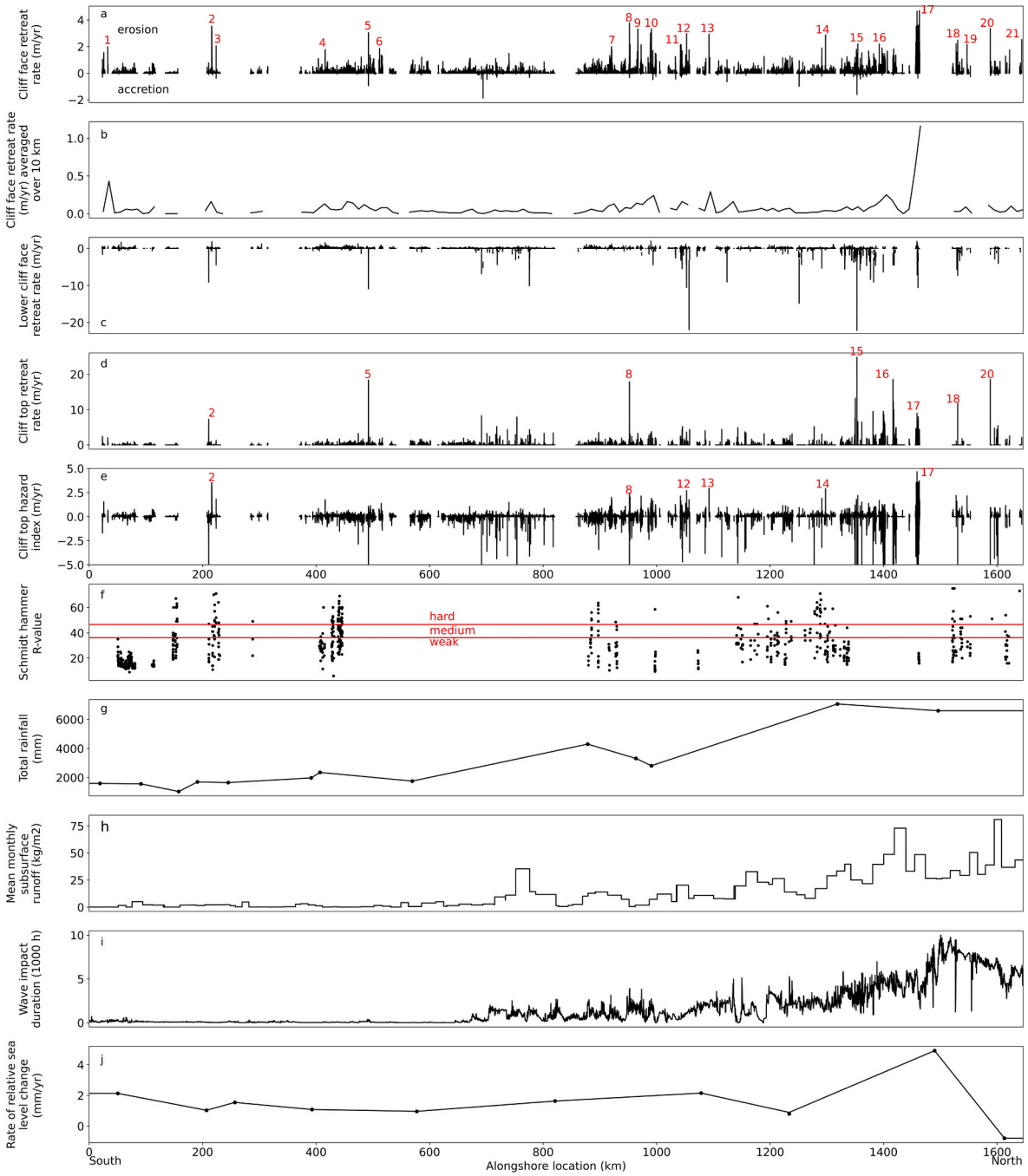

Fig. 4. Alongshore distribution of California coastal cliff changes between 2009–2011 and 2016 including a) cliff face retreat rate; b) cliff face retreat rate averaged over 10 km alongshore blocks; c) lower cliff face (≤4.7 m NAVD88) retreat rate; d) cliff top retreat rate and e) cliff top hazard index. Negative values in panels a and c indicate net accretion (deposition). Alongshore distribution of environmental factors including f) Schmidt hammer rebound value (red lines delimit weak, medium, and hard rocks classified using Hoek and Brown (1997) with uniaxial compressive strength (UCS) calculated using Eq. (1)), r) total rainfall, h) groundwater conditions, i) wave impact duration for an idealized cliff base at 2.5 m NAVD88, and j) rate of relative sea level change trend (tidesandcurrents.noaa.gov). 0 km and 1646 km represent the Mexico (south) and Oregon (north) borders. Erosional hotspots: 1 – Sunset Cliffs, 2 – Portuguese Bend, 3 – Palos Verdes, 4 – Haskell's Beach, 5–2.3 km south of Point Arguello, 6 – Vandenberg, 7 – Año Nuevo State Park, 8 – Martin's Beach, 9 – Miramar, 10 – Pacifica, 11 – Bolinas, 12 – Double Point, 13 – Point Reyes, 14 – Caspar Beach, 15 – Usal Beach, 16 – King Range, 17 – Centerville Beach, 18 – Trinidad Head, 19 – Humboldt Lagoon State Park, 20 – 3 km north of Klamath River, 21 – Clifford Kampf Memorial Park. (For interpretation of the references to colour in this figure legend, the reader is referred to the web version of this article.)

northward, ranging between 483 and 4729 mm. Mean total rainfall was 1714 mm in southern, 2673 mm in central, and 4375 mm in northern California (Fig. 4g).

The mean monthly modeled subsurface runoff ranged from 0 to 81 kg m^{-2}, and varied spatially with a mean of 1 kg m^{-2} for southern, 7 kg m^{-2} for central, and 32 kg m^{-2} for northern California (Fig. 4h). The maximum monthly modeled subsurface runoff ranged from 0 to 540 kg m^{-2}, and also generally increased northward. Subsurface runoff was spatially correlated with total rainfall (r^2 = 0.6–0.7; $p < 0.05$).

All wave impact metrics varied spatially, and generally increased northward (Fig. 4i). For example, the estimated wave impact duration between 2009–2011 and 2016 ranged from 0 to 6601 h and varied by

Table 1
Summary of cliff changes for California regions and counties. Values are mean ± standard deviation.

Region/ county	Alongshore extent (km)	Time period 3 analyzed cliff length (km)	Armored cliffs (%)	Cliff height (m)	Cliff face retreat rate (m yr^{-1})		Cliff top retreat rate (m yr^{-1})			Schmidt hammer R-value[a]
					Time period 2	Time period 3	Time period 1	Time period 2	Time period 3	
Northern CA	1132–1646	264	1.5	61 ± 55	–	0.08 ± 0.25	0.39 ± 0.42	–	0.10 ± 0.67	34 ± 13
Central CA	420–1132	415	7.1	37 ± 33	0.05 ± 0.17	0.05 ± 0.16	0.29 ± 0.32	0.13 ± 0.27	0.05 ± 0.28	25 ± 12
Southern CA	0–420	187	20	25 ± 16	0.03 ± 0.08	0.05 ± 0.13	0.19 ± 0.22	0.12 ± 0.19	0.03 ± 0.16	27 ± 14
Del Norte	1576–1646	21	4.9	67 ± 56	–	0.05 ± 0.20	0.41 ± 0.28	–	0.10 ± 1.03	30 ± 13
Humboldt	1382–1576	69	0.2	79 ± 58	–	0.18 ± 0.42	0.78 ± 0.44	–	0.23 ± 0.86	32 ± 14
Mendocino	1209–1382	128	0.7	59 ± 55	–	0.05 ± 0.13	0.37 ± 0.43	–	0.06 ± 0.71	35 ± 14
Sonoma	1126–1209	48	4.1	36 ± 38	0.01 ± 0.01	0.05 ± 0.06	0.20 ± 0.18	0.31 ± 0.38	0.02 ± 0.15	35 ± 11
Marin	1015–1126	52	2.2	63 ± 41	0.07 ± 0.17	0.09 ± 0.22	0.53 ± 0.42	0.21 ± 0.41	0.05 ± 0.25	18 ± 6
San Francisco	996–1015	5	21	42 ± 25	0.16 ± 0.37	0.16 ± 0.29	–	1.08 ± 1.00	0.12 ± 0.35	21 ± 14
San Mateo	915–996	62	7.4	30 ± 33	0.09 ± 0.25	0.11 ± 0.29	0.31 ± 0.38	0.16 ± 0.29	0.10 ± 0.41	26 ± 10
Santa Cruz	853–915	48	24	23 ± 14	0.04 ± 0.08	0.03 ± 0.07	0.15 ± 0.12	0.09 ± 0.14	0.04 ± 0.13	32 ± 12
Monterey	686–853	116	5.2	47 ± 33	0.01 ± 0.06	0.02 ± 0.07	0.40 ± 0.37	0.13 ± 0.26	0.03 ± 0.26	–
San Luis Obispo	546–686	88	4.1	21 ± 23	0.04 ± 0.07	0.03 ± 0.08	0.19 ± 0.16	0.05 ± 0.14	0.03 ± 0.12	–
Santa Barbara	370–546	119	12	25 ± 19	0.05 ± 0.08	0.07 ± 0.11	0.19 ± 0.16	0.11 ± 0.15	0.06 ± 0.28	38 ± 13
Ventura	303–370	1	49	19 ± 8	0.00 ± 0.02	0.06 ± 0.08	0.19 ± 0.22	–	0.03 ± 0.08	–
Los Angeles	187–303	35	13	38 ± 15	0.02 ± 0.10	0.05 ± 0.23	0.30 ± 0.35	0.09 ± 0.15	0.02 ± 0.31	37 ± 15
Orange	120–187	16	28	20 ± 11	0.01 ± 0.03	0.00 ± 0.01	0.14 ± 0.15	0.09 ± 0.15	0.00 ± 0.02	39 ± 13
San Diego	0–120	57	27	25 ± 20	0.02 ± 0.08	0.03 ± 0.08	0.15 ± 0.22	0.15 ± 0.23	0.01 ± 0.07	16 ± 3
California	0–1646	866	8.2	42 ± 41	0.04 ± 0.14	0.06 ± 0.19	0.26 ± 0.31	0.12 ± 0.24	0.06 ± 0.46	29 ± 14

[a] Available for total 66 km.

Table 2
Summary of cliff retreat for different cliff classes and time periods. Retreat values are mean ± standard deviation.

Property	Class	Cliff length (km)	Retreat rate (m yr^{-1})
Cliff face retreat			
Armoring	Armored	71	0.03 ± 0.14
	Unarmored	795	0.06 ± 0.19
Beach	With beach	403	0.08 ± 0.23
	Without beach	463	0.04 ± 0.13
Rock hardness	Hard	9.4	0.04 ± 0.11
	Medium	10	0.04 ± 0.07
	Weak	47	0.08 ± 0.23
Time	Time period 2	595	0.04 ± 0.14
	Time period 2 overlapping with time period 3	402	0.06 ± 0.16
Cliff top retreat			
Time	Time period 1	353	0.26 ± 0.31
	Time period 1 overlapping with time period 3	274	0.24 ± 0.29
	Time period 2	236	0.12 ± 0.24
	Time period 2 overlapping with time period 3	214	0.12 ± 0.23

more than an order of magnitude between northern and southern California (Fig. 4i), with a mean of 62 h for southern, 1111 h for central, and 3387 h for northern California (Fig. 4i). The three wave impact metrics were strongly correlated ($r^2 > 0.96$, $p < 0.05$).

The RSL trend at most tide stations ranges about 1–2 mm yr^{-1}, but deviates in North Spit, Eureka (1490 km) with a trend of 4.9 mm yr^{-1}, while the Crescent City station (1613 km) shows decreasing water levels of −0.79 mm yr^{-1} (Fig. 4j).

4.5. Relationships between cliff erosion and environmental factors

Correlations between the rate of unarmored cliff face erosion, and the individual explanatory variables – rock hardness, rainfall, groundwater, wave impact metrics, and RSL change – at 5 m scale were all weak ($r^2 < 0.05$, $p < 0.05$). Similarly, lower cliff erosion rates and wave impact metrics were not well correlated ($r^2 < 0.05$). At the largest spatial scale evaluated using alongshore smoothing (100 km) correlations between cliff face erosion rates and explanatory variables increased to $r^2 =$ 0.1–0.14 ($p < 0.05$) for rock hardness, mean and maximum subsurface runoff, and wave impact metrics, and to $r^2 = 0.29$ ($p < 0.05$) for RSL. Despite weak correlations between spatial variability in cliff erosion rates and individual environmental factors, cliffs with the highest cliff face retreat rates (>1 m yr^{-1}) generally had low (<25) R-values (Fig. 7a). Additional analysis of multivariable, nonlinear correlations, and cliff subgroups (e.g. cliffs classified by height or slope) did not yield any significant results.

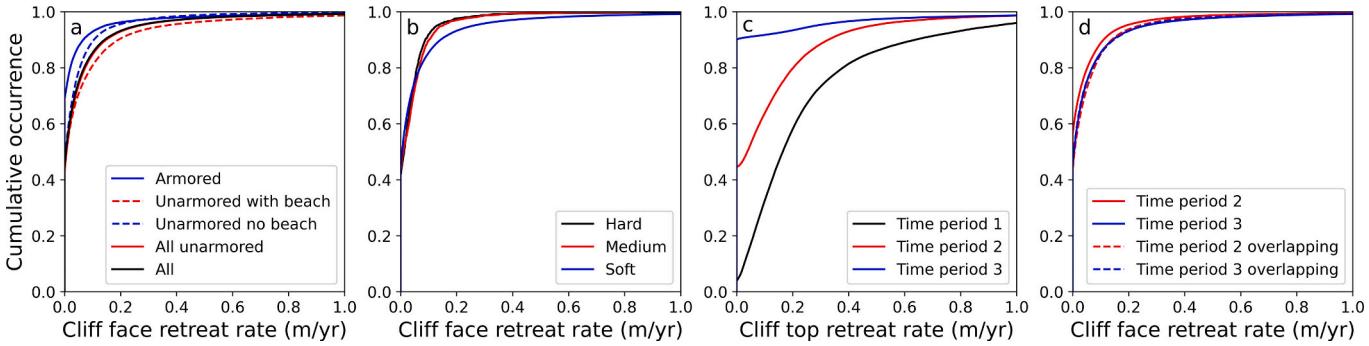

Fig. 5. Cumulative occurrence of cliff face retreat rates depending on a) armoring and presence of a beach fronting the cliff, and b) rock hardness. Cumulative occurrence of the c) cliff top retreat rates for time period 1 (1920s–1930s to 1998/2002), time period 2 (1998 to 2009–2011), and time period 3 (2009–2011 to 2016), and d) cliff face retreat rates for time periods 2 and 3 for all locations (solid lines) and only location with spatial overlap (dash lines). For display purposes x-axes are limited to 1 m yr^{-1}.

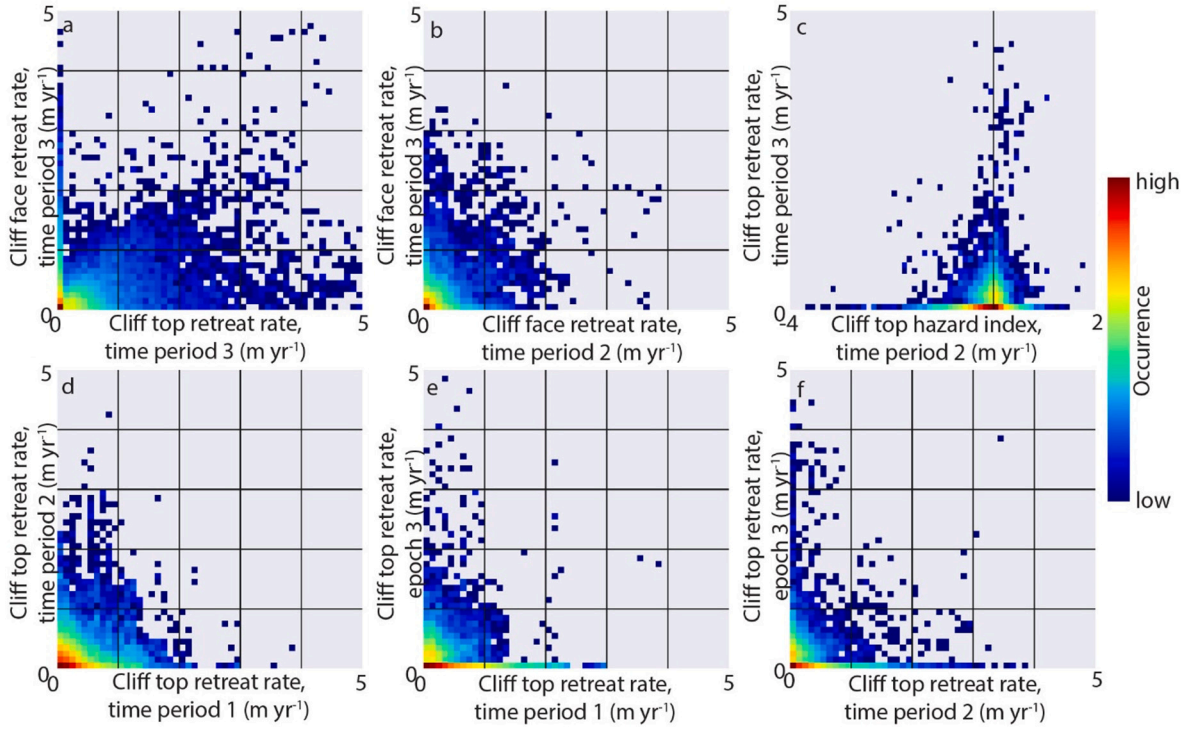

Fig. 6. Density plots of a) cliff top and face retreat rates in time period 3, b) cliff face retreat rates in time period 2 and 3, c) cliff top hazard index in time period 2 and cliff top retreat rates in time period 3, and cliff top retreat for time periods d) 1 and 2, e) 1 and 3, and f) 2 and 3. All values are in 0.1 m yr^{-1} bins. Compartments with cliff top retreat rate $\geq$ 5 m yr^{-1} in time period 3 (n = 188) are beyond the axis limits.

5. Discussion

This study provides the largest high-resolution analysis of California cliff erosion to date and includes detailed analysis for ~500 km of the coast not previously examined (mostly in northern California). Between 2009–2011 and 2016, the average cliff face and top retreat rates were similar, but the cliff top erosion rates were more diverse (0.46 vs 0.19 m yr^{-1} standard deviation). More compartments experienced zero cliff top retreat compared to zero cliff face retreat (90% vs 45%, Fig. 5c, vertical strip in Fig. 6a), for which we suggest two possible explanations. First, the cliff face often erodes with high-frequency low-magnitude events, while cliff top failures occur more episodically (Lim et al., 2010; Rosser et al., 2013; Williams et al., 2018). Second, the change detection methods used for each metric are different – while cliff face change detection used vertical and area-based thresholds, the cliff top retreat detection uses a direct minimum retreat threshold (1 m for this study; Swirad and Young, 2022). Additionally, the highest cliff top retreat rates are larger than the highest cliff face retreat rates (25 vs 4.7 m yr^{-1}; Fig. 4a and d). Abnormally high cliff top retreat can also occur on complex shorelines where the primary direction of cliff retreat is not perpendicular to the primary shoreline (and compartment) orientation. The lower number of cliff top retreat events suggests that the relative stability of the cliff top may lead to a false indication of overall cliff stability (Lim et al., 2010). Observed erosional hotspots (Fig. 4a and d) with cliff retreat rates 30–400 times greater than the statewide average highlight the highly localized and episodic nature of large coastal cliff failures.

We observed that hard and medium hardness rock cliffs retreated slower than those with weak rocks (Fig. 7a). A global compilation (Prémaillon et al., 2018) of local studies found mean retreat rates of 0.03 $\pm$ 0.03 m yr^{-1} for hard, 0.10 $\pm$ 0.08 m yr^{-1} for medium and 0.23 $\pm$ 0.25 m yr^{-1} for weak rock cliffs (median $\pm$ median absolute deviation). Our

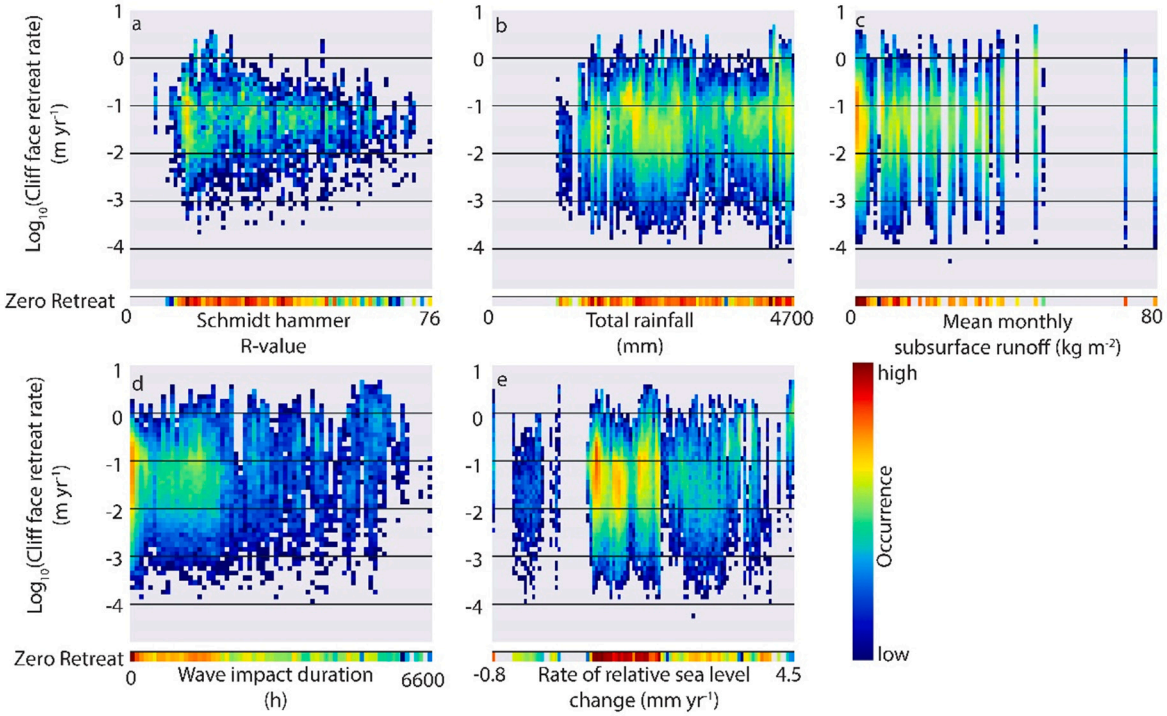

Fig. 7. Density distribution of the environmental factors and cliff face retreat rates using 0.05 m yr^{-1} bins: a) Schmidt hammer rebound value (1 R-value bins); b) total rainfall (50 mm bins); c) groundwater conditions (1 kg m^{-2} bins); d) wave impact duration (100 h bins); e) rate of relative sea level change (0.05 mm yr^{-1} bins). Plots use a log scale y-axis to increase data visibility, but this precludes plotting bins with zero retreat; zero retreat bins are shown in the horizontal strips below each panel.

results are within these ranges. Moreover, our density distribution suggests that the highest erosion rates usually occurred in relatively weak rocks (Fig. 7a), an intuitive pattern that has been numerically modeled (Walkden and Hall, 2005; Walkden and Dickson, 2008; Limber et al., 2014).

The observation that cliffs fronted by beaches retreated twice as fast as those without beaches is consistent with the findings of Young (2018). This finding is counterintuitive, because wide beaches can protect cliffs from wave action. However, waves can also use beach sand as an abrasive to erode the lower cliff (Robinson, 1977; Sunamura, 1982; Kline et al., 2014). Numerical modelling suggests that beach material concentrates in bays which form at weaker cliff sections (Limber et al., 2014), where weaker rocks have higher retreat rates. The finding may also reflect a trend found elsewhere, that exposed rocky headlands experience lower erosion because the rocks are harder and rock platforms are generally higher at headlands, limiting wave-cliff interaction (So, 1965; Kirk, 1977). Future studies should explore the spatial distribution of additional cliff settings such as areas with shore platforms and plunging cliffs, and examine their differences in cliff retreat rates.

The average and the statistical distribution of cliff top retreat rates vary considerably between the three study time periods. Direct comparison is complicated because of the different types and quality of data sources used, and variable mapping methods (manual vs automated). However, time period 1 cliff top retreat rates were more evenly statistically distributed, suggesting that longer (~70 year) time periods average out the stochastic nature of cliff failure and the system moves towards spatially uniform retreat rates in time (Young, 2018).

Although not correlated at the compartment level, cliff face retreat rates in time periods 2 and 3 have similar statistical distributions (Fig. 5a) despite the different study timespans and time periods. Additionally, when only overlapping compartments are considered, the average cliff face retreat rate for time periods 2 and 3 were similar.

The mismatch between cliff top retreat rates for the three time periods indicates that estimating future change from observed cliff retreat rates at specific locations could be problematic. However, the consistent cliff face retreat distributions in time periods 2 and 3 show a probabilistic approach to retreat prediction could be more successful. Swirad and Young (2021) showed that the time period 3 landslide size distribution closely followed the power law, which would also help facilitate a probabilistic prediction approach.

High time period 2 cliff top hazard indices did not correlate well with increased cliff retreat in time period 3 in many locations. This could result from the inability of the short timespan (~6 years) of time period 3 to capture longer (decadal) term cliff top retreat processes and cycles, and suggests the hazard may still persist. In addition, high time period 2 cliff face retreat rates in some areas may be related to erosion of landslide deposits rather than new bedrock erosion. Also, the hazard index is a relative value applicable to a specific location where steepening leads to cliff top collapse, and is not directly comparable to other cliff sections with different geologic/morphologic settings. The hazard index may not work for locations where cliff top failure is unrelated to steepening.

Despite higher mean erosion rates in northern California compared to central and southern California, and the general trend of increasing northward wave energy, rainfall, and subsurface runoff (Fig. 4), it remains difficult to directly link coastal cliff erosion with environmental factors. The lack of observed relationships could be related to differences in the spatial and temporal resolution of the datasets and the studied timespan that may not resolve the complex processes at various spatio-temporal scales. For example, the LiDAR datasets have very high spatial resolution but provide only the start and end morphology. Conversely, the environmental data had higher temporal resolution (hourly for waves; daily for rainfall; monthly for runoff) or were considered time-independent (rock hardness and RSL trend), and had varied spatial resolution. In addition, other processes and factors such as wind, beach elevation, and local event-scale rainfall, which can all influence cliff erosion, were not included.

Higher temporal resolution assessment of topographic change may provide better linkages between cliff failures, specific rainfall events,

and wave impact metrics (Young et al., 2021). Higher temporal resolution assessment of topographic change would also provide a detailed time series of back beach elevation, and allow better estimates of wave impact parameters. New satellite-based observations of beach change (e.g. Vos et al., 2020) could potentially help improve wave impact metrics for regions with otherwise sparse beach observations. However, further development is needed to measure beach elevations at the cliff base from satellite-based observations and to validate wave impact metrics.

Rock hardness was only measured at limited areas of the California cliffs (~4.5%) and additional observations could be useful. Improvements to rock characterization should also include methods to measure the rock hardness of very weak rocks (<10 MPa), unattainable with the present tools, and consider additional factors such as lithology and discontinuities at varied spatial scales that influence resistance to erosion (Budetta et al., 2000; Dickson et al., 2004). Finally, Eq. (1) may be too simplistic to derive UCS from Schmidt hammer measurements, given the diversity of lithologies and state of weathering of California cliffs.

Compilations of cliff erosion rates allow the general comparison of how erosion varies between regions and geology types (Sunamura, 1992; Prémaillon et al., 2018). Numerical modelling allows better understanding of the mechanisms and feedbacks of cliff erosion, but model parameters are often abstract and hence difficult to apply for real situations, while explored timelines tend to be beyond the managerial (annual to decadal) scope (Kline et al., 2014; Limber et al., 2014; Matsumoto et al., 2016). Cosmogenic radionuclide dating can help calibrate and validate cliff erosion models and better understand how short-term erosion rates measured in the field feed into long-term cliff evolution patterns (Regard et al., 2012; Hurst et al., 2016; Swirad et al., 2020). However, the variability in cliff erosion at the local to regional scale (10^0–10^5 m) remains difficult to model because of diversity in coastal settings (e.g. topography, geology, wave climate, rainfall pattern, stage of cliff development). This study confirms the complexity of processes and persisting lack of datasets that are needed to constrain drivers of coastal cliff retreat. We advocate for nested studies which are needed to understand how changes during single storm/rainfall events (Young et al., 2021) propagate in time over years/decades (present study) and how this reflects the long-term (centuries/millennia) evolution of a rocky coast.

6. Conclusions

Coastal cliff erosion was measured at 5 m resolution along 866 km of coastal cliffs in California between 2009–2011 and 2016. Erosion was detected at 55% cliffs. Cliff face retreat rates averaged 0.06 ± 0.19 m yr^{-1} (mean ± std. dev) and cliff top retreat rates averaged 0.06 ± 0.43 m yr^{-1} (mean ± std. dev), and varied alongshore with higher rates in northern California compared to central and southern California. The retreat rates were twice as high for unarmored cliffs compared to armored, and those fronted by beaches compared to cliffs without beaches, consistent with previous research. Erosional hotspots included Palos Verdes, ~2.3 km south of Point Arguello, Big Sur, Martin's Beach, Usal Beach, King Range, Centerville Beach, McNeil Creek area north of Trinidad Head, and ~3 km north of the Klamath River. Portuguese Bend, Martin's Beach, Point Reyes, Double Point, Caspar Beach, and Centerville Beach had relatively high cliff top hazard indices, indicating cliff steepening.

Cliff top retreat rates between 2009–2011 and 2016 were lower than that measured over an earlier period of ~70 years using historical maps, and that measured for a preceding ~12-year period, which may be a methodical artifact. However, mean and statistical distribution of cliff face retreat rates were similar to those measured using similar techniques in the preceding ~12-year time period.

Wave impact, rainfall, groundwater conditions, and cliff retreat rates were higher in northern California compared to southern California, and many of the locations with the highest retreat rates were locations with weak rocks. However, no spatial correlations were identified between rates of cliff retreat and individual environmental factors, highlighting the complexity and variability of processes acting on the California coast.

Declaration of competing interest

The authors declare that they have no known competing financial interests or personal relationships that could have appeared to influence the work reported in this paper.

Acknowledgements

The study was funded by the California Ocean Protection Council (C0303100) administered by University of Southern California Sea Grant and the California Department of Parks and Recreation, Natural Resources Division Oceanography Program (C1670004 and C19E0049). We are grateful to Esther Essoudry (California Coastal Commission) for sharing the armoring data, Patrick Limber for sharing Schmidt hammer measurements, Hironori Matsumoto for helping in the field, Jessica Carilli for manuscript proofreading, and the editor and two anonymous reviewers for constructive comments.

References

ASTM, 2013. C805/C805M-13a Standard Test Method for Rebound Number of Hardened Concrete. ASTM International, West Conshohocken, PA, USA.
Barlow, J., Lim, M., Rosser, N., Petley, D., Brain, M., Norman, E., Geer, M., 2012. Modeling cliff erosion using negative power law scaling of rockfalls. Geomorphology 139–140, 416–424.
Barnard, P.L., Hoover, D., Hubbard, D.M., Snyder, A., Ludka, B.C., Allan, J., Kaminsky, G. M., Ruggiero, P., Gallien, T.W., Gabel, L., McCandless, D., 2017. Extreme oceanographic forcing and coastal response due to the 2015–2016 El Niño. Nat. Commun. 8 (1), 1–8.
Brooks, S.M., Spencer, T., Boreham, S., 2012. Deriving mechanisms and thresholds for cliff retreat in soft-rock cliffs under changing climates: Rapidly retreating cliffs of the Suffolk coast, UK. Geomorphology 153–154, 48–60.
Budetta, P., Galietta, G., Santo, A., 2000. A methodology for the study of the relation between coastal cliff erosion and the mechanical strength of soils and rock masses. Eng. Geol. 56 (3–4), 243–256.
Collins, B.D., Sitar, N., 2008. Processes of coastal bluff erosion in weakly lithified sands, Pacifica, California, USA. Geomorphology 97 (3–4), 483–501.
Dickson, M.E., Kennedy, D.M., Woodroffe, C.D., 2004. The influence of rock resistance on coastal morphology around Lord Howe Island, Southwest Pacific. Earth Surf. Process. Landf. 29 (5), 629–643.
Dickson, M.E., Walkden, M.J.A., Hall, J.W., 2007. Systemic impacts of climate change on an eroding coastal region over the twenty-first century. Clim. Chang. 84, 141–166.
Emery, K.O., Kuhn, G.G., 1982. Sea cliffs: their processes, profiles, and classification. Geol. Soc. Am. Bull. 93 (7), 644–654.
Evans, B., 2015. Mar 26. Woman Dies in Bluff Collapse at Arch Rock. Point Reyes Light.
Griggs, G., Patsch, K., Savoy, L., 2005. Living With the Changing California Coast. University of California Press, Berkeley, CA, USA.
Gross, G., Davis, K., 2008. August 21. Beach-goer dies after cliff collapses. In: The San Diego Union Tribune.
Hapke, C.J., Reid, D., Richmond, B., 2009. Rates and trends of coastal change in California and the regional behavior of the beach and cliff system. J. Coast. Res. 25 (3), 603–615.
Hapke, C.J., Adams, P.N., Allan, J., Ashton, A., Griggs, G.B., Hampton, M.A., Kelly, J., Young, A.P., 2014. The rock coast of the USA. In: Memoirs 40, Chapter 9. Geological Society, London, pp. 137–154.
Hoek, E., Brown, E.T., 1997. Practical estimates of Rock Mass Strength. Int. J. Rock Mech. Min. Sci. 34, 1165–1186.
Hurst, M.D., Rood, D.H., Ellis, M.A., Anderson, R.S., Dornbusch, U., 2016. Recent acceleration in coastal cliff retreat rates on the south coast of Great Britain. Proc. Natl. Acad. Sci. U. S. A. 113 (47), 13336–13341.
Jennings, C.W., 1977. Geologic Map of California. Department of Conservation, Division of Mines and Geology, State of California, Sacramento, California.
Katz, O., Reches, Z., Roegiers, J.C., 2000. Evaluation of mechanical rock properties using a Schmidt hammer. Int. J. Rock Mech. Min. Sci. 37, 723–728.
Kirk, R.M., 1977. Rates and forms of erosion on intertidal platforms at Kaikoura Peninsula, South Island, New Zealand. N. Z. J. Geol. Geophys. 20, 571–613.
Kline, S.W., Adams, P.N., Limber, P.W., 2014. The unsteady nature of sea cliff retreat due to mechanical abrasion, failure and comminution feedbacks. Geomorphology 219, 53–67.
Lim, M., Rosser, N.J., Allison, R.J., Petley, D.N., 2010. Erosional processes in the hard rock coastal cliffs at Staithes, North Yorkshire. Geomorphology 114, 12–21.
Limber, P.W., Murray, A.B., Adams, P.N., Goldstein, E.B., 2014. Unraveling the dynamics that scale cross-shore headland relief on rocky coastlines: 1. Model development.

J. Geophys. Res. Earth Surf. 119 (4), 854–873. https://doi.org/10.1002/2013JF002950.
Ludka, B.C., Gallien, T.W., Crosby, S.C., Guza, R.T., 2016. Mid-El Niño erosion at nourished and unnourished Southern California beaches. Geophys. Res. Lett. 43 (9), 4510–4516.
Matsumoto, H., Dickson, M.E., Kench, P.S., 2016. An exploratory numerical model of rocky shore profile evolution. Geomorphology 268, 98–109.
Naylor, L.A., Stephenson, W.J., 2010. On the role of discontinuities in mediating shore platform erosion. Geomorphology 114, 89–100.
Naylor, L.A., Stephenson, W.J., Trenhaile, A.S., 2010. Rock coast geomorphology: recent advances and future research directions. Geomorphology 114 (1–2), 3–11.
O'Reilly, W.C., Olfe, C.B., Thomas, J., Seymour, R.J., Guza, R.T., 2016. The California coastal wave monitoring and prediction system. Coast. Eng. 116, 118–132.
Perry, T., 2000. January 16. Landslide Kills Woman as She Watches Husband Surf. Los Angeles Times.
Prémaillon, M., Regard, V., Dewez, T.J.B., Auda, Y., 2018. GlobR2C2 (global recession rates of coastal cliffs): a global relational database to investigate coastal rocky cliff erosion rate variations. Earth Surf. Dyn. 6, 651–668.
Regard, V., Dewez, T., Bourlès, D.L., Anderson, R.S., Duperret, A., Costa, S., Leanni, L., Lasseur, E., Pedoja, K., Maillet, G.M., 2012. Late Holocene seacliff retreat recorded by 10Be profiles across a coastal platform: theory and example from the English Channel. Quat. Geochronol. 11, 87–97.
Reichenbach, P., Rossi, M., Malamud, B.D., Mihir, M., Guzzetti, F., 2018. A review of statistically-based landslide susceptibility models. Earth-Sci. Rev. 180, 60–91.
Robinson, L.A., 1977. Marine erosive processes at the cliff foot. Mar. Geol. 23 (3), 257–271.
Rosser, N.J., Brain, M.J., Petley, D.N., Lim, M., Norman, E.C., 2013. Coastline retreat via progressive failure of rocky coastal cliffs. Geology 41, 939–942.
Smith, S.A., Barnard, P.L., 2021. The impacts of the 2015/2016 El Niño on California's sandy beaches. Geomorphology 377, 107583.
So, C.L., 1965. Coastal platforms of the Isle of Thanet, Kent. Trans. Inst. Br. Geogr. 147–156.
Stockdon, H.F., Holman, R.A., Howd, P.A., Sallenger Jr., A.H., 2006. Empirical parameterization of setup, swash, and runup. Coast. Eng. 53, 573–588.
Sunamura, T., 1982. A wave tank experiment on the erosional mechanism at a cliff base. Earth Surf. Process. Landf. 7, 333–343.
Sunamura, T., 1992. Geomorphology of Rocky Coasts. John Wiley & Son Ltd.
Swirad, Z.M., Young, A.P., 2021. Automating coastal cliff erosion measurements from large-area LiDAR datasets in California, USA. Geomorphology 389, 107799.
Swirad, Z.M., Young, A.P., 2022. CliffDelineaTool v1.2.0: an algorithm for identifying coastal cliff base and top positions. Geosci. Model Dev. 15, 1499–1512.
Swirad, Z.M., Rosser, N.J., Brain, M.J., Rood, D.H., Hurst, M.D., Wilcken, K.M., Barlow, J., 2020. Cosmogenic exposure dating reveals limited long-term variability in erosion of a rocky coastline. Nat. Commun. 11, 3804.
Thomas, M.A., Loague, K., 2014. Devil's slide: an evolving feature of California's coastal landscape. Environ. Eng. Geosci. 20 (1), 45–65.
Trenhaile, A.S., 1987. The Geomorphology of Rock Coasts. Oxford University Press.
USACE, 2015. In: Coastal Engineering Manual – Part II. EM 1110-2-1100 (Part II). 30 September 2015 (Change 4). Engineering and Design. U.S. Army Corps of Engineers, Washington, DC, p. 623.
Vos, K., Harley, M.D., Splinter, K.D., Walker, A., Turner, I.L., 2020. Beach slopes from satellite-derived shorelines. Geophys. Res. Lett. 47 (14), e2020GL088365.
Walkden, M., Dickson, M., 2008. Equilibrium erosion of soft rock shores with a shallow or absent beach under increased sea level rise. Mar. Geol. 251, 75–84.
Walkden, M.J.A., Hall, J.W., 2005. A predictive mesoscale model of the erosion and profile development of soft rock shores. Coast. Eng. 52, 535–563.
Warrick, J.A., Ritchie, A.C., Schmidt, K.M., Reid, M.E., Logan, J., 2019. Characterizing the catastrophic 2017 Mud Creek landslide, California, using repeat structure-from-motion (SfM) photogrammetry. Landslides 16, 1201–1219.
Williams, J.G., Rosser, N.J., Hardy, R.J., Brain, M.J., Afana, A.A., 2018. Optimising 4-D surface change detection: an approach for capturing rockfall magnitude–frequency. Earth Surf. Dyn. 6, 101–119.
Young, A.P., 2015. Recent deep-seated coastal landsliding at San Onofre State Beach, California. Geomorphology 228, 200–212.
Young, A.P., 2018. Decadal-scale coastal cliff retreat in southern and Central California. Geomorphology 300, 164–175.
Young, A.P., Carilli, J.E., 2019. Global distribution of coastal cliffs. Earth Surf. Process. Landf. 44, 1309–1316.
Young, A.P., Flick, R.E., Gutierrez, R., Guza, R.T., 2009. Comparison of short-term seacliff retreat measurement methods in Del Mar, CA. Geomorphology 112, 318–323.
Young, A.P., Guza, R.T., O'Reilly, W.C., Hansen, J.E., Barnard, P.L., 2011. Short-term retreat statistics of a slowly eroding coastal cliff. Nat. Hazards Earth Syst. Sci. 11, 205–217.
Young, A.P., Flick, R.E., Gallien, T.W., Giddings, S.N., Guza, R.T., Harvey, M., Lenain, L., Ludka, B.C., Melville, W.K., O'Reilly, W.C., 2018. Southern California coastal response to the 2015–2016 El Niño. J. Geophys. Res. Earth Surf. 123 (11), 3069–3083.
Young, A.P., Guza, R.T., Matsumoto, H., Merrifield, M.A., O'Reilly, W.C., Swirad, Z.M., 2021. Three years of weekly observations of coastal cliff erosion by waves and rainfall. Geomorphology 375, 107545.